Eur. Phys. J. A **9**, 261–267 (2000)

THE EUROPEAN PHYSICAL JOURNAL A

Nuclear effects and higher twists in F_3 structure function

S.A. Kulagin[1,a] and A.V. Sidorov[2]

[1] Institute for Nuclear Research of the Russian Academy of Sciences, 117312 Moscow, Russia
[2] Bogoliubov Laboratory of Theoretical Physics, Joint Institute for Nuclear Research, 141980 Dubna, Russia

Received: 4 August 2000
Communicated by W. Weise

Abstract. We analyze the CCFR collaboration iron target data on the xF_3 structure function making particular emphasis on the extraction of the higher twist contributions from the data. Corrections for nuclear effects are applied in order to extract data on the structure function of the isoscalar nucleon. Our analysis confirms the observation made earlier, that the higher twist terms depend strongly on the level to which QCD perturbation theory analysis is applied. We discuss the impact of nuclear effects on the higher twist term as well as on the QCD scale parameter $\Lambda_{\overline{MS}}$ extracted from the fit to data.

PACS. 12.38.Bx Perturbative calculations – 13.85.Hd Inelastic scattering: many-particle final states – 21.60.-n Nuclear-structure models and methods – 24.85.+p Quarks, gluons, and QCD in nuclei and nuclear processes

1 Introduction

In the present paper we report the results of our analysis of the CCFR collaboration data [1] on the structure function xF_3. The particular emphasis of the analysis is to constrain the higher twist (HT) contributions to the structure function from the data. The HT effects in the xF_3 structure function are of particular interest because of certain theoretical predictions made in the framework of infrared renormalon technique [2–5]. An attempt to constrain the HT terms from the CCFR/NuTeV collaboration data was done in [6,7], where the F_3 structure function was written as the sum of two terms,

$$xF_3(x,Q^2) = xF_3^{\rm LT}(x,Q^2) + \frac{h(x)}{Q^2}, \qquad (1)$$

with $F_3^{\rm LT}$ the leading twist contribution and h/Q^2 the HT term. An important observation which follows from the analysis [6–8] is that the magnitude of the HT term depends on the level to which the perturbation theory analysis of $F_3^{\rm LT}$ is applied. If $F_3^{\rm LT}$ is evaluated in a leading order (LO) renormalization group formalism a large $h(x)$ appears from the fit. When a next-to-leading order (NLO) formalism is used for $F_3^{\rm LT}$ a somewhat smaller but still substantial contribution from the HT term is needed. If $F_3^{\rm LT}$ is evaluated to next-to-next-to-leading order (NNLO) very little room is left for the HT term.

We note that QCD analysis of data implies that data are given for isolated proton and neutron. In practice, due to the reason of statistics, neutrino data are taken mainly on nuclear targets rather than on isolated proton and neutron. For example, the CCFR/NuTeV collaboration uses the iron target, the IHEP-JINR Neutrino Detector uses the aluminum target [9], and the forthcoming data from CHORUS collaboration is obtained on the lead target [10]). It is known from muon and electron DIS experiments, that nuclear effects are quite essential in a wide kinematical region of x and Q^2 (the EMC effect at large x, nuclear shadowing at small x, for a review see, *e.g.*, [11]). Therefore, the separation of nuclear effects from data introduces certain corrections to QCD analysis of data.

All these motivate us to make a new analysis of the CCFR neutrino data taking into account corrections due to nuclear effects. Our analysis involves two steps. In section 2 we discuss our approach to calculate nuclear structure functions and to correct data for nuclear effects, and then in section 3 we report the results of QCD analysis of corrected data. In sect. 4 we summarize.

2 Nuclear structure functions

In order to apply corrections for nuclear effects in our analysis we first calculate the "EMC ratio" for the iron target, $R_3(x,Q^2) = F_3^A(x,Q^2)/AF_3^N(x,Q^2)$, with F_3^A the structure function of a heavy nucleus of A nucleons and F_3^N the structure function of an isolated isoscalar nucleon[1]. Then we extract the structure function of an isolated isoscalar nucleon from the CCFR data, $F_3^N(x,Q^2) = F_3^{\rm CCFR}(x,Q^2)/R_3(x,Q^2)$.

[a] e-mail: kulagin@ms2.inr.ac.ru

[1] The isoscalar nucleon structure function is defined as $F_3^N = \frac{1}{2}(F_3^p + F_3^n)$.

Bulk of neutrino data with $Q^2 > 1\,\mathrm{GeV}^2$ is located in the region of $x > 0.1$. For this kinematical regime it is usually assumed that nuclear DIS of leptons from nuclear targets can be viewed as incoherent scattering from bound nucleons. Major nuclear effects found in this region are due to nuclear binding [12] and Fermi motion [13] and off-shell modification of bound nucleon structure functions [14]. For the simplest nuclear system, the deuteron, the relation between the deuteron and the nucleon F_3 structure function reads as follows [15]:

$$xF_3^D(x,Q^2) = 2\int \frac{\mathrm{d}^3\boldsymbol{p}}{(2\pi)^3}\,|\Psi_D(\boldsymbol{p})|^2 \times \left(1+\frac{p_z}{\gamma M}\right) x' F_3^N(x',Q^2;p^2), \quad (2)$$

where $\Psi_D(\boldsymbol{p})$ is the deuteron wave function which describes the probability to find the bound proton (or neutron) with momentum $\boldsymbol{p}$, $x' = Q^2/2p{\cdot}q$ is the Bjorken variable of the bound nucleon with the four-momentum p which is given by the difference of the target four-momentum and the four-momentum of the spectator nucleon. Equation (2) is written for the target rest frame and the axis z is chosen along the direction of momentum transfer, $q = (q_0, 0_\perp, -|\boldsymbol{q}|)$. In this reference frame $p = (M_D - \sqrt{\boldsymbol{p}^2 + M^2}, \boldsymbol{p})$ with M_D and M the deuteron and the nucleon mass, respectively, and $\gamma = |\boldsymbol{q}|/q_0 = (1 + 4x^2M^2/Q^2)^{1/2}$ is the "velocity" of the virtual boson. Note that the bound proton and neutron are off-mass-shell and their structure functions depend on the nucleon off-shellness p^2 as an additional variable.

For the scattering off a heavy nucleus of A nucleons, there appears a rich spectrum of spectator nuclear states of $A-1$ nucleons, over which we have to sum. The nuclear structure function is then given by equation similar to (2) where we have to substitute the deuteron wave function by nuclear spectral function $\mathcal{P}(\varepsilon,\boldsymbol{p})$ and introduce an additional integration over the energy spectrum of spectator states [15],

$$xF_3^A(x,Q^2) = \sum_{\tau=p,n}\int \frac{\mathrm{d}\varepsilon\,\mathrm{d}^3\boldsymbol{p}}{(2\pi)^4}\,\mathcal{P}^\tau(\varepsilon,\boldsymbol{p}) \times \left(1+\frac{p_z}{\gamma M}\right) x' F_3^\tau(x',Q^2;p^2), \quad (3)$$

where the sum is over protons ($\tau = p$) and neutrons ($\tau = n$). The nucleon four-momentum $p = (M+\varepsilon, \boldsymbol{p})$. The proton and neutron spectral functions, $\mathcal{P}^p$ and $\mathcal{P}^n$, are normalized to the number of bound protons (Z) and neutrons (N), respectively.

Heavy nuclei, such as iron $^{56}\mathrm{Fe}_{26}$, generally have got unequal numbers of protons and neutrons with an excess of the latter over the former. The neutron excess is generally small, $(N-Z)/A \ll 1$. Therefore, it is a good approximation to assume that the neutron and the proton spectral functions calculated per one particle are equal, $\mathcal{P}^p/Z = \mathcal{P}^n/N$. Then we find from (3),

$$xF_3^A = \left\langle \left(1+\frac{p_z}{\gamma M}\right)\left(x'F_3^N + \frac{N-Z}{2A}\,(x'F_3^n - x'F_3^p)\right)\right\rangle, \quad (4)$$

where the averaging is done with respect to the isoscalar spectral function, $\mathcal{P}^p+\mathcal{P}^n$. The last term in (4) gives a correction due to excess of neutrons in a nucleus. We notice that the sign of this correction is different for neutrino and anti-neutrino scattering. Indeed, we have $F_3^\nu = 2(d-\bar{u})$ with d and u the parton distributions of corresponding quarks in the target (we neglect for simplicity the contributions due to s- and c-quarks). Since the neutron has more d-quarks than the proton has (in the valence quark region), the neutrino-neutron structure function is larger than the proton one, $F_3^{\nu n} > F_3^{\nu p}$. Therefore $F_3^{\nu A}$ receives a positive correction due to excess of neutrons. Repeating this argument for anti-neutrino scattering, we find that the corresponding correction is equal in magnitude but opposite in sign (*i.e.* negative). Therefore the $N-Z$ correction vanishes for the structure function averaged over neutrino and antineutrino. Similar discussion can also be applied to the F_2 structure function. One can also see that the $N-Z$ correction is negative for the charged leptons scattering, *i.e.* for the $F_2^{\mu A}$ structure function.

As it is obvious from (3), calculation of nuclear structure functions requires the knowledge of nuclear spectral function. In the next section we discuss the nuclear spectral function used in the present calculation in more detail.

2.1 Nuclear spectral function

Nuclear spectral function $\mathcal{P}$ determines the probability to find the nucleon with the momentum $\boldsymbol{p}$ and (non relativistic) energy ε in the ground state of the nucleus and can be written as follows:

$$\mathcal{P}(\varepsilon,\boldsymbol{p}) = 2\pi\sum_{n,\sigma}|\langle (A-1)_n, -\boldsymbol{p}\,|a_\sigma(\boldsymbol{p})|\,A\rangle|^2 \times \delta\left(\varepsilon + E_n^{A-1} + \frac{\boldsymbol{p}^2}{2M_{A-1}} - E_0^A\right). \quad (5)$$

Here the sum is over the quantum numbers of the whole set of the residual states of $A-1$ nucleons which includes the bound states as well as the sates in continuum, $a_\sigma(\boldsymbol{p})$ is the annihilation operator of the nucleon with momentum $\boldsymbol{p}$ and polarization σ, and E_n^{A-1} and E_0^A are, respectively, the energy of the residual nucleus and the ground-state energy of the target nucleus. The residual system balances momentum of the removed nucleon and acquires the recoil energy $\boldsymbol{p}^2/2M_{A-1}$ though its effect is small for heavy nuclei. The nuclear momentum distribution is

$$n(\boldsymbol{p}) = \int \frac{\mathrm{d}\varepsilon}{2\pi}\,\mathcal{P}(\varepsilon,\boldsymbol{p}). \quad (6)$$

The integration of the spectral function over energy and momentum gives the number of bound nucleons A.

The spectral function (5) determines the rate of nucleon removal reactions such as $A(e,e'p)X$ that makes it possible to extract the spectral function from experimental data[2]. The picture of the spectrum of residual states as

[2] Though one should notice, that the direct connection between the cross-sections and the spectral function holds only

revealed from these experiments with heavy nuclei can be summarized as follows. At low energies and momentum [3] the energy spectrum of residual states follows to that predicted by the mean-field model of the nucleus, *i.e.* it consists of the set of sharp peaks whose positions can be identified with the energies needed to separate bound nucleons from the occupied single particle levels in the nuclear mean field. The deviations from the mean-field picture become significant at high momentum $\boldsymbol{p}$ and high nucleon removal energy ε. The widths of the resonances increase as ε increases as well as the positions of the peaks move from that predicted by the energy independent mean-field model. At high energy the spectral function is dominated by contributions from the states with one and more nucleons in the continuum. These contributions are due to NN-correlations in the nuclear ground state and cannot be accounted for within the mean-field model.

2.1.1 Phenomenological model of spectral function

The calculation of the nuclear spectral function for complex nuclei requires to solve many-body problem. The latter is known to be a difficult task and presently can be done only within certain approximations. In our discussion we follow [16] and consider a phenomenological model for the spectral function which incorporates both the single-particle nature of the spectrum at low energy as well as high-energy and high-momentum components due to NN-correlations in the ground state[4]. To this end, we separate the full spectral function (5) into two parts,

$$\mathcal{P}(\varepsilon,\boldsymbol{p}) = \mathcal{P}_0(\varepsilon,\boldsymbol{p}) + \mathcal{P}_1(\varepsilon,\boldsymbol{p}), \tag{7}$$

which correspond to contributions from low-excitation energy intermediate states ($\mathcal{P}_0$) and high-excitation energy states ($\mathcal{P}_1$). The low-energy part can be approximated by the sum of the energy δ-functions which pick the positions of the occupied single-particle levels weighted with the corresponding wave functions squared. In practice we use an approximate expression instead, where the sum over occupied levels is substituted by its average value,

$$\mathcal{P}_0(\varepsilon,\boldsymbol{p}) = 2\pi\, n_0(\boldsymbol{p})\delta\left(\varepsilon + E^{(1)} + \frac{\boldsymbol{p}^2}{2M_{A-1}}\right), \tag{8}$$

with $E^{(1)} = E^{A-1} - E_0^A$ the nucleon separation energy averaged over residual configurations of $A-1$ nucleons with low excitation energies, *i.e.* mean-field configurations, and $n_0(\boldsymbol{p})$ the corresponding part of the nucleon momentum distribution.

The high-energy part $\mathcal{P}_1$ is determined by excited states in (5) with one or more nucleons in the continuum. It was observed within many-body calculations [17,16] for a wide range of nuclei that nuclear momentum distributions at high momenta ($|\boldsymbol{p}| > p_{\rm F}$ with $p_{\rm F}$ the Fermi momentum) run parallel to the deuteron distribution $n_D(\boldsymbol{p})$,

$$n_1(\boldsymbol{p}) \approx C^A n_D(\boldsymbol{p}), \tag{9}$$

where the normalization constant C^A incorporates the many-body aspects of the problem. It was found [16] that the constants C^A increase from 2 for ^{3}He to 4.5 for ^{56}Fe. Going to a larger mass number does not bring any longer to a high momentum component, $C^A = 5$ for nuclear matter[5].

This observation finds a simple interpretation if one assumes that the high momentum component is generated by ground-state configurations with a correlated NN-pair with a small distance between the nucleons. One can expect therefore that the relative motion in the NN-pair is determined by the properties of the NN-interaction in the vacuum rather than by long-range nuclear interactions, and the distribution in the relative momentum will be similar to momentum distribution in the deuteron.

In terms of the spectral function $\mathcal{P}_1$ this corresponds to the assumption about the dominance of the contribution from the states with one nucleon in the continuum and the remaining $A-2$ nucleons being in a state with low momentum and low excitation energy,

$$|A-1,-\boldsymbol{p}\rangle \approx a^\dagger(\boldsymbol{p}_1)|(A-2)^*,\boldsymbol{p}_2\rangle\delta(\boldsymbol{p}_1+\boldsymbol{p}_2+\boldsymbol{p}). \tag{10}$$

The coprresponding matrix element in (5) is then determined by the wave function of the NN-pair embeded into nuclear environment,

$$\langle (A-2)^*,\boldsymbol{p}_2\,|a(\boldsymbol{p}_1)a(\boldsymbol{p})|\,A\rangle = \psi_{\rm rel}(\boldsymbol{k})\psi^{A-2}_{\rm CM}(\boldsymbol{p}_{\rm CM})\delta(\boldsymbol{p}_1+\boldsymbol{p}_2+\boldsymbol{p}). \tag{11}$$

We assume here factorization into the wave functions describing the relative motion in the NN pair, $\psi_{\rm rel}(\boldsymbol{k})$, with relative momentum $\boldsymbol{k} = (\boldsymbol{p}-\boldsymbol{p}_1)/2$ and the center-of-mass (CM) motion of the pair in the field of $A-2$ nucleons, $\psi^{A-2}_{\rm CM}(\boldsymbol{p}_{\rm CM})$ with $\boldsymbol{p}_{\rm CM} = \boldsymbol{p}_1 + \boldsymbol{p}$. In general $\psi_{\rm CM}$ depends on the quantum numbers of the state of $A-2$ nucleons, however the corresponding dependence of the $\psi_{\rm rel}$ is weak.

We substitute (11) into (5) and sum over the spectrum of $A-2$ nucleons states and obtain an approximate expression for $\mathcal{P}_1$,

$$\mathcal{P}_1(\varepsilon,\boldsymbol{p}) = (2\pi)\int \mathrm{d}^3\boldsymbol{p}_1\mathrm{d}^3\boldsymbol{p}_{\rm CM} n_{\rm rel}(\boldsymbol{k}) n_{\rm CM}(\boldsymbol{p}_{\rm CM}) \times \delta(\boldsymbol{p}_1+\boldsymbol{p}-\boldsymbol{p}_{\rm CM})\,\delta\left(\varepsilon+\frac{\boldsymbol{p}_1^2}{2M}+\frac{\boldsymbol{p}_{\rm CM}^2}{2M_{A-2}}+E^{(2)}\right). \tag{12}$$

Here $n_{\rm rel}$ and $n_{\rm CM}$ are the relative and the CM momentum distributions, respectively, and $E^{(2)} = E^{A-2} - E_0^A$ is the

in the impulse approximation, and is destroyed by other effects such as final-state interactions and meson exchange currents.

[3] The momenta should be compared with Fermi momentum $p_{\rm F}$ which is for heavy nuclei $p_{\rm F} \approx 300\,$MeV/c. The corresponding Fermi energy is of order $\varepsilon_{\rm F} \approx 40$ MeV.

[4] We note that our definition of the spectral function is different from the one used in [16], where the recoil energy was not included into the energy δ-function in (5).

[5] One should note however, that relation (9) does not hold at low momentum where $n_1(\boldsymbol{p})$ contributes only a little to the full momentum distribution.

energy needed to separate two-nucleons from the ground state averaged over configurations of $A-2$ nucleons with low excitation energy. Note that the minimum two nucleon separation energy $E^{(2)} = E_0^{A-2} - E_0^A$ is of order of 20 MeV for medium-range nuclei like ^{56}Fe.

The factorization of the matrix element (11) into the relative and the CM motion wave functions is justified if relative momentum in the NN-pair is large relative to the CM momentum of the pair. This can be written as $|\boldsymbol{p}| \gg |\boldsymbol{p}_{\rm CM}|$. This condition allows us to approximate (12) by taking the relative momentum distribution out of the integral over the CM momentum at the point $\boldsymbol{k} = \boldsymbol{p}$. Then we have,

$$\mathcal{P}_1(\varepsilon, \boldsymbol{p}) = (2\pi) n_{\rm rel}(\boldsymbol{p}) \times \left\langle \delta\left(\varepsilon + \frac{(\boldsymbol{p}+\boldsymbol{p}_2)^2}{2M} + \frac{\boldsymbol{p}_2^2}{2M_{A-2}} + E^{(2)}\right)\right\rangle_{\rm CM}, \quad (13)$$

where the averaging is done with respect to the CM motion of the pair. From the latter equation it is clear that the high-momentum part of nuclear momentum distribution is given by the relative momentum distribution in the correlated NN-pair embedded in the nuclear environment, $n_1(\boldsymbol{p}) = n_{\rm rel}(\boldsymbol{p})$.

The characteristic momentum for the CM motion of the NN-pair is similar to the one in the mean-field model. In fact the averaged CM momentum squared of the pair can be estimated from the balance of the overall nucleus momentum [16], $\langle(\sum \boldsymbol{p}_i)^2\rangle = 0$, where the sum is taken over all bound nucleons and the averaging is performed with respect to the intrinsic wave function of the nucleus. This gives $\langle \boldsymbol{p}_{\rm CM}^2\rangle = 2(A-2)\langle \boldsymbol{p}^2\rangle/(A-1)$, with $\langle \boldsymbol{p}^2\rangle$ the mean value of the squared single-nucleon momentum. Since, by our assumption, the CM distribution does not include the high-momentum component, we should also exclude the contribution of the high-momentum part in estimating $\langle \boldsymbol{p}^2\rangle$. We follow [16] and parameterize the CM momentum distribution of the correlated NN pair in the field of other $A-2$ nucleons by a Gaussian distribution,

$$n_{\rm CM}(\boldsymbol{p}_{\rm CM}) = (\alpha/\pi)^{3/2} \exp(-\alpha \boldsymbol{p}_{\rm CM}^2), \quad (14)$$

with the parameter α determined from the averaged CM momentum of the pair, $\alpha = 3/(2\langle \boldsymbol{p}_{\rm CM}^2\rangle)$.

Using (14) we find that the integration over the CM momentum in (13) can be done analytically and finally the result reads,

$$\mathcal{P}_1(\varepsilon, \boldsymbol{p}) = n_1(\boldsymbol{p}) \frac{2M}{|\boldsymbol{p}|} \sqrt{\alpha\pi} \left(\exp(-\alpha p_{\rm min}^2) - \exp(-\alpha p_{\rm max}^2)\right), \quad (15)$$

where $p_{\rm min}$ and $p_{\rm min}$ are respectively the minimum and the maximum CM momenta allowed by the energy-momentum conservation in (12) for the given ε and $\boldsymbol{p}$,

$$p_{\rm max}^2 = \left(\frac{A-2}{A-1}|\boldsymbol{p}| + p_T\right)^2, \quad p_{\rm min}^2 = \left(\frac{A-2}{A-1}|\boldsymbol{p}| - p_T\right)^2, \quad (16)$$

$$\text{with} \quad p_{\rm T} = \left(\frac{A-2}{A-1}\left(-2M(\varepsilon + E^{(2)}) - \frac{\boldsymbol{p}^2}{A-1}\right)\right)^{1/2}.$$

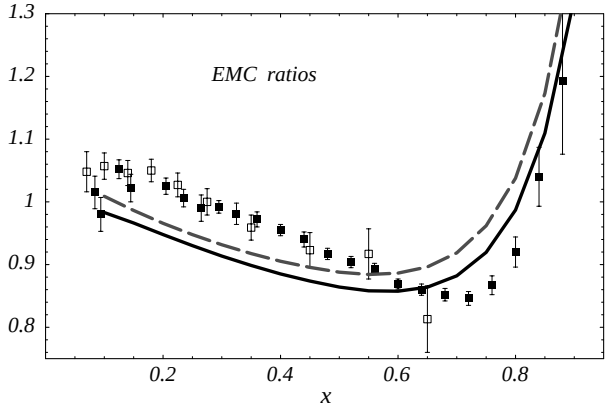

Fig. 1. The iron/deuterium ratios (EMC ratios) calculated for the structure functions F_2 (solid curve) and F_3 (dashed curve) within the model described in the text. The data points are from BCDMS [18] (open boxes) and SLAC [19] (filled boxes) experiments. The curves were calculated at fixed $Q^2 = 16\,{\rm GeV}^2$ using CTEQ4 parameterizations for the nucleon parton distributions.

We notice that $p_{\rm T}$ has the interpretation of the maximal allowed CM momentum in the correlated NN-pair in the direction transverse to $\boldsymbol{p}$ for the fixed ε and $|\boldsymbol{p}|$. Note that the separation energy ε is negative, as follows from its definition in (5). The condition $p_{\rm T}^2 = 0$ determines the threshold value of ε for the fixed $|\boldsymbol{p}|$.

In numerical evaluations we use the parameterizations for $n_0(\boldsymbol{p})$ and $n_1(\boldsymbol{p})$ of [16], which fit nicely the results of many-body calculation of nuclear momentum distribution. It follows from this calculation that low momentum part incorporates about 80% of the total normalization of the spectral function while the other 20% are taken by the high-momentum part. The mean kinetic energy obtained from integration of the full momentum distribution $n_0 + n_1$ for the iron nucleus is $\langle \boldsymbol{p}^2\rangle/2M = 31\,{\rm MeV}$ (the share of the high-momentum component n_1 is about 20 MeV). The two parameters, $E^{(1)}$ and $E^{(2)}$, determine the characteristic range of nucleon separation energy. We set $E^{(2)} = E_0^{A-2} - E_0^A = 20\,{\rm MeV}$, and therefore neglect possible contributions due to excited states of $A-2$ nucleons in (12)[6]. In order to fix the parameter $E^{(1)}$ we employ the Koltun sum rule [20], which gives the relation between mean separation energy $\langle\varepsilon\rangle$, mean kinetic energy $\langle \boldsymbol{p}^2\rangle/2M$, and the ground-state energy per nucleon E_0^A/A. For the mean kinetic energy of 31 MeV the sum rule gives $\langle\varepsilon\rangle \approx -50\,{\rm MeV}$. By integrating our model spectral function we find the value $E^{(1)} = 27\,{\rm MeV}$ which satisfies the Koltun sum rule.

[6] The effect of $A-2$ excited states would lead to an overall increase of nucleon separation energy. We believe, however, that concrete estimates of this effect would require that we go beyond the model discussed in the present paper.

2.2 The EMC ratios R_2 and R_3

In fig.1 we compare the iron/deuterium ratios for the charged lepton structure function F_2^μ and the neutrino and antineutrino averaged structure function F_3, calculated with the model nuclear spectral function discussed above. Also shown are the BCDMS [18] and the SLAC [19] data on the iron/deuterium F_2 structure function ratios. In numerical calculations we use the CTEQ4 parameterizations for the nucleon parton distributions [21]. We see that the behavior of the ratio R_3 is very similar to that of the ratio R_2 (for large x and large Q^2 this does not come as a big surprise, since both F_2 and xF_3 are determined by valence quarks in this region). A small difference between the R_2 and R_3 curves is due to the neutron excess correction. As was discussed in sect. 1, the F_2^μ structure function receives a negative $N-Z$ correction, while similar correction cancels out in the neutrino and antineutrino averaged structure functions. It is well known, that the depletion of nuclear structure functions at $x < 0.7$ is due to nuclear binding effect [12], while the rise of the ratios at large $x > 0.7$ is due to nuclear momentum distribution effect (Fermi motion).

We recall also that bound nucleons are off-mass-shell. Off-shell effects in the structure functions appear as the dependence on the target invariant mass p^2. Target mass corrections can be of two different kinds. First of all, we have to take into account "kinematical" target mass dependence due to finite p^2/Q^2 ratio. To this end we use the Nachtmann scaling variable [22] $\xi = 2x'/(1 + (1 + 4x'^2p^2/Q^2))^{1/2}$ instead of the Bjorken variable x'. Other ("dynamical") sources of p^2-dependence of structure functions are also possible. In this respect we refer to a model where p^2-dependence of structure functions appears in the leading order [14,15]. We note also here, that we take into account off-shell effects in the bound nucleon structure function in a way that it does not affect the number of valence quarks in the nucleon [15]. The off-shell effect acts coherently with nuclear binding effect and leads to an additional suppression of nuclear structure functions at intermediate range of x.

The ratio R_2 follows quite closely to data on the EMC effect in the iron nucleus (see fig. 1). This gives us the confidence in our method to calculate the EMC effect in the F_3 structure function.

3 QCD analysis and fit

Our QCD fit proceeds as follows. The nucleon structure function $F_3^N(x, Q^2)$ is written as a sum of the leading twist and the high twist terms, (1). We parametrize $xF_3^{\rm LT}$ at some scale $Q^2 = Q_0^2$ in terms of a simple function,

$$xF_3^{\rm LT}(x, Q_0^2) = a_1 x^{a_2}(1-x)^{a_3}(1 + a_4 x). \qquad (17)$$

Then we apply the renormalization group equation in order to calculate evolution of $xF_3^{\rm LT}$ with Q^2. We solve the renormalization group equation in the leading (LO), next-to-leading (NLO) and next-to-next-to-leadig (NNLO) logarithm approximations of QCD. In doing so, we expand the leading twist structure function $xF_3^{\rm LT}$ in terms of its Mellin moments within the framework of the Jacobi polinomial method and then apply the evolution equations to the moments (for more detail on the method used see [23]).

It should be noticed that in general the higher twist terms can be of two kinds: those which have the kinematical nature, *e.g.* the terms due to finite target mass, and those which arise due to higher twist operators and reflect the quark-gluon interaction effects in the target ("pure" higher twists). In order to ensure that the higher twist term in (1) describes effects due to quark-gluon interaction in the target we explicitly take into account the kinematical corrections due to finite target mass. To this end we substitute the Mellin moments by the Nachtmann moments [22] in the the Jacobi polinomial expansion of the leading twist structure function $xF_3^{\rm LT}$.

The CCFR data points are given in terms of discrete x-bins structure which range from $x = 0.0075$ to $x = 0.75$. We fit 116 data points with Q^2 in the range between $1.3\,{\rm GeV}^2$ and $200\,{\rm GeV}^2$. The fit parameters are the parameters a_2, a_3, and a_4 of (17) at the scale Q_0^2, the values of the function $h(x_i)$ at the center of each x_i-bin, as well as the QCD scale parameter $\Lambda_{\overline{MS}}$. We fix the parameter a_1 by normalizing (17) to the Gross-Llewellyn-Smith sum rule, which was calculated in QCD to the second order in α_S [24], $S_{\rm GLS} = 3(1 - \alpha_S/\pi - 3.25(\alpha_S/\pi)^2)$.

Our results are shown in fig. 2 for the LO, NLO and NNLO approximations to the evolution equation. Also shown are the results with and without applying corrections for nuclear effects. We found that the fitting parameters are stable for $Q_0^2 > 15\,{\rm GeV}^2$ and have chosen $Q_0^2 = 20\,{\rm GeV}^2$ for the results presented in fig. 2. The present fit includes more experimental points than that of [6,7]. In particular, the inclusion of low-Q^2 data points into the fit allows us to reduce the error bars in $h(x)$ as compared to those presented in [6,7]. Though we should notice some increasing theoretical uncertainties associated with low Q^2 data included into our analysis. We found that, in general, our present fit agrees with [6,7], though introduces certain corrections especially at large x.

A special care was taken to insure that our method to separate target mass correction is self-consistent. In particular we have done a special fit with $h(x_i)$ fixed at values presented in fig. 2, but let the mass parameter in the Nachtmann moments to be free. We found that the minimum of χ^2 corresponds to the value of the mass parameter about $0.9\,{\rm GeV}$ with an error about $0.2\,{\rm GeV}$. This value only weakly depends on the order of perturbative analysis and is close to the proton mass, that gives us confidence in the method used.

As one can clearly see from fig. 2 the magnitude of the higher twist effects depends on the level to which the perturbation theory analysis of $F_3^{\rm LT}$ is done. The more perturbative corrections are included into the evolution equation, the less room is left for the function $h(x)$. The shape of $h(x)$ in NLO is in a qualitative agreement with the prediction of infrared renormalon approach [3]. In par-

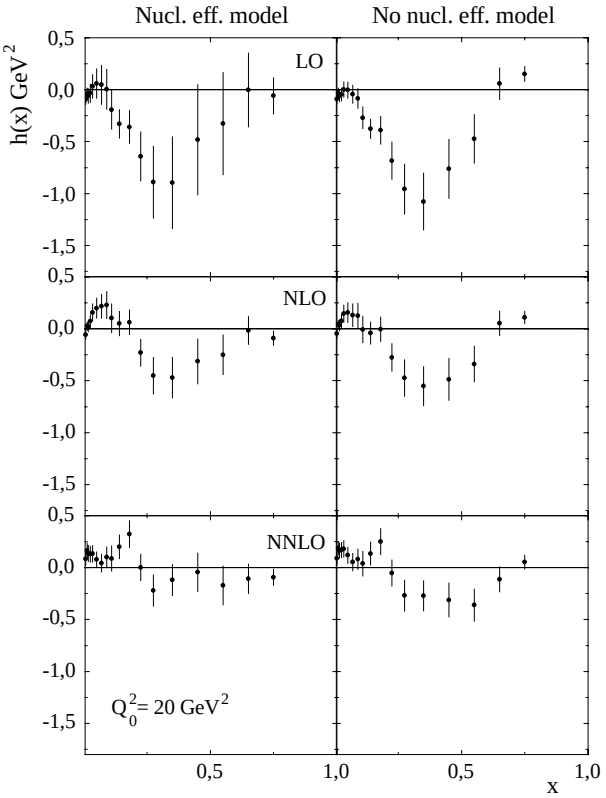

Fig. 2. The function $h(x)$, which describes the strength of the higher twist term in the xF_3 structure function as extracted from the fit to the CCFR neutrino data (see text). The labels on the figure indicate the level to which the perturbation theory analysis of $xF_3^{\rm LT}$ is done.

ticular, we found that the function $h(x)$ is negative in the region $0.1 < x < 0.6$.

The separation of nuclear effects from data leads to a further suppression of the higher twist term $h(x)$ at all levels of perturbation theory analysis of $F_3^{\rm LT}$. The effect of nuclear corrections on $h(x)$ is most pronounced at large x, where we observe a systematic reduction of $h(x)$ as compared with no-nuclear-effects analysis. Nuclear corrections result in the decrease of the values of the function $h(x)$ at $x > 0.6$. As one can see from fig. 2, the central points of $h(x)$ at $x = 0.65$ and $x = 0.75$ bins become negative in contrast to the infrared renormalon prediction for large x [3]. An attempt to take into account nuclear effects in the QCD fit was previously done in [25,7]. We comment in this respect that authors of [25] used the deuteron model for nuclear effects, which is not a realistic one for the iron target. In particular, we found that $h(x)$ is negative for large x, while it was positive in [25]. Authors of [7] attempted to introduce nuclear corrections to QCD fit in terms of the moments of structure functions. However, it was incorrectly assumed in [7], that the nuclear structure function $F_3^A \to 0$ as $x \to 1$, that, to our mind, caused the χ^2 increase in their QCD fit.

We found that the scale parameter $\Lambda_{\overline{MS}}$ decreases for about 40 MeV after nuclear effects are taken into account. This will lead to a shift of $\alpha_S(M_Z)$ for about $2 \cdot 10^{-3}$. Within the NNLO fit we get $\Lambda_{\overline{MS}} = (394 \pm 55)$ MeV for four quark flavors.

4 Summary and conclusions

In the present paper we report the results of our QCD analysis of CCFR data on F_3 structure function. The main emphasis was put on the extraction of higher twist contribution from the data. We took special care to separate nucler effects from the data, and compare the results of both analyses with and without corrections for nuclear effects.

We found that nuclear effects cause about 10% decrease in the $\Lambda_{\overline{MS}}$ value.

Our analysis confirms the observation made earlier, that the magnitude of higher twist terms decreases strongly when going from LO to NLO, and then to NNLO, approximations to the evolution equation. We observe an additional suppression of higher twist terms when corrections due to nuclear effects have been applied.

In conclusion we note that small-x region in F_3 structure function is of particular interest, where a strong nuclear shadowing effect is anticipated [26]. We plan to address nuclear shadowing effect in application to QCD analysis of neutrino data.

This work was supported in part by the RFBR project no. 00-02-17432. We are grateful to A.L. Kataev for useful discussions.

References

1. W.G. Seligman, Columbia Univ, Thesis R-1257, CU-368, Nevis-292, 1997; CCFR-NuTeV Collab., W.G. Seligman et al., *Phys. Rev. Lett.* **79**, 1213 (1997).
2. M. Beneke and V.M. Braun, *Phys. Lett.* B **348**, 513 (1995); Yu. L. Dokshitzer, G. Marchesini and B.R. Webber, *Nucl. Phys.* B **469**, 93 (1996).
3. M. Dasgupta and B.R. Webber, *Phys. Lett.* B **382**, 273 (1996); M. Maul, E. Stein, A. Schäfer and L. Mankiewicz, *Phys. Lett.* B **401**, 100 (1997).
4. M. Beneke, *Phys. Rept.* **317**, 1 (1999).
5. F.V. Gubarev, M.I. Polikarpov and V.I. Zakharov. Lectures given at *27th ITEP Winter School of Physics, Moscow, 16-24 Feb 1999.* Preprint ITEP-TH-36-99 (1999), [hep-ph/9908292].
6. A.L. Kataev, A.V. Kotikov, G. Parente and A.V. Sidorov, *Phys. Lett.* B **417**, 374 (1998).
7. A.L. Kataev, G. Parente, and A.V. Sidorov, *Nucl. Phys.* B **573**, 405 (2000).
8. A.V. Sidorov, *Phys. Lett.* B **389**, 379 (1996).
9. IHEP-JINR Neutrino Detector Collab., A.V. Sidorov et al., *Nucl. Phys. B (Proc. Suppl.)* **79**, 99 (1999); *Eur. Phys. J.* C **10**, 405 (1999).
10. R.G.C. Oldeman for the CHORUS collab., *Nucl. Phys. B (Proc. Suppl.)* **79**, 96 (1999).
11. M. Arneodo, *Phys. Rep.* **240**, 301 (1994).
12. S.V. Akulinichev, S.A. Kulagin, and G.M. Vagradov, *Phys. Lett.* B **158**, 485 (1985); S.V. Akulinichev, S. Shlomo, S.A. Kulagin, and G.M. Vagradov, *Phys. Rev. Lett.* **55**, 2239 (1985); S.A. Kulagin, *Nucl. Phys.* A **500**, 653 (1989).

13. G.B. West, *Ann. Phys.* **74**, 464 (1972).
14. S.A. Kulagin, G. Piller and W. Weise, *Phys. Rev.* C **50**, 1154 (1994).
15. S.A. Kulagin, *Nucl. Phys.* A **640**, 435 (1998).
16. C. Ciofi degli Atti and S. Simula, *Phys. Rev.* C **53**, 1689 (1996).
17. J.G. Zabolitsky and W. Ey, *Phys. Lett.* B **76**, 527 (1978).
18. A.C. Benvenuti *et al., Phys. Lett.* B **189**, 483 (1985).
19. J. Gomez *et al., Phys. Rev.* D **49**, 4348 (1994).
20. D.S. Koltun, *Phys. Rev.* C **9**, 484 (1974).
21. H.L. Lai *et al.*, *Phys. Rev.* D **55**, 1280 (1997).
22. O. Nachtmann, *Nucl. Phys.* B **63**, 237 (1973); S. Wandzura, *Nucl. Phys.* B **122**, 412 (1977).
23. G. Parisi and N. Sourlas, *Nucl. Phys.* B **151**, 421 (1979); I.S. Barker, C.B. Langensiepen, and G. Shaw, *Nucl. Phys.* B **186**, 61 (1981); V.G. Krivokhizhin *et al., Z. Phys.* C **36**, 51 (1987); C **48**, 347 (1990); A.L. Kataev and A.V. Sidorov, *Phys. Lett.* B **331**, 179 (1994).
24. S.G. Gorishny and S.A. Larin, *Phys. Lett.* B **172**, 109 (1986).
25. M.V. Tokarev and A.V. Sidorov, *Nuovo Cim.* A **110**, 1401 (1997).
26. S.A. Kulagin, hep-ph/9812532.